Available online at www.sciencedirect.com
SCIENCE DIRECT®
Journal of Magnetic Resonance 181 (2006) 287–295
JMR Journal of Magnetic Resonance
www.elsevier.com/locate/jmr

Water absorption kinetics in different wettability conditions studied at pore and sample scales in porous media by NMR with portable single-sided and laboratory imaging devices

V. Bortolotti [a], M. Camaiti [b], C. Casieri [c,d,*], F. De Luca [c,e], P. Fantazzini [f], C. Terenzi [c,e]

[a] *Dipartimento DICMA, Università di Bologna, V.le Risorgimento 2, I-40126 Bologna, Italy*
[b] *CNR-ICVBC, V. Madonna del Piano 10, I-50019 Sesto Fiorentino, Firenze, Italy*
[c] *Research center SOFT-INFM-CNR, Università "La Sapienza", P.le Aldo Moro 2, I-00185 Roma, Italy*
[d] *Dipartimento di Fisica, Università di L'Aquila, V. Vetoio 10, I-67010 Coppito, L'Aquila, Italy*
[e] *Dipartimento di Fisica, Università "La Sapienza", P.le Aldo Moro 2, I-00185 Roma, Italy*
[f] *Dipartimento di Fisica, Università di Bologna, V.le Berti Pichat 6/2, I-40127 Bologna, Italy*

Received 16 March 2006; revised 23 May 2006
Available online 19 June 2006

Abstract

NMR relaxation time distributions of water ^{1}H obtained by a portable single-sided surface device have been compared with MRI internal images obtained with a laboratory imaging apparatus on the same biocalcarenite (Lecce Stone) samples during capillary water uptake. The aim of this work was to check the ability of NMR methods to quantitatively follow the absorption phenomenon under different wettability conditions of the internal pore surfaces. Stone wettability changes were obtained by capillary absorption of a chloroform solution of Paraloid PB72, a hydrophobic acrylic resin frequently used to protect monuments and buildings, through one face of each sample. Both relaxation and imaging data have been found in good quantitative agreement each other and with masses of water determined by weighing the samples. In particular the Washburn model of water capillary rise applied to the imaging data allowed us to quantify the *sorptivity* in both treated and untreated samples. Combining relaxation and imaging data, a synergetic improvement of our understanding of the water absorption kinetics at both pore and sample scales is obtained. Since relaxation data have been taken over the course of time without interrupting the absorption process, simply by keeping the portable device on the surface opposite to the absorption, the results show that the single-sided NMR technique is a powerful tool for *in situ* evaluation of water-repellent treatments frequently used for consolidation and/or protection of stone artifacts.

Keywords: Single-sided NMR; NMR imaging; Porous media; Hydrophobic treatment; Capillary hydration kinetics; T_2 distribution function

1. Introduction

The characterization of the internal structure and fluid transport properties of porous building materials is essential for evaluating the state of conservation of historical-artistic items, for planning appropriate restoration and conservation, and for determining the durability and efficacy of consolidation and/or protective treatments. As porous materials (i.e., concrete, mortar, stone, travertine or marble) can absorb or release water in response to environmental conditions, their properties are greatly affected by moisture content. Moreover, water is also the principal degradation agent in this wide range of materials that are exposed to moisture and air pollutants. Trapped water can dissolve and transport pollutants that make soluble or corrode the components of the media, altering their porosity and/or causing micro-fractures. Therefore, the knowledge of capillary properties and porosity is essential for the evaluation of the conservation state of building materials, and suitable non-destructive diagnostic techniques are required.

* Corresponding author. Fax: +39 0862 43 3033.
E-mail address: cinzia.casieri@aquila.infn.it (C. Casieri).

1090-7807/$ - see front matter © 2006 Elsevier Inc. All rights reserved.
doi:10.1016/j.jmr.2006.05.016

The use of water molecules to explore the pore space makes NMR techniques appropriate for applications in the field of porous media [1].

Magnetic relaxation of ^{1}H nuclei of water confined in porous media has been widely employed during the last decades as a powerful tool for investigation of structural properties of high surface-to-volume ratio (S/V) systems. Since the proton NMR signal from the sample is proportional to the total amount of water entrapped in the pore space, the analysis of the proton relaxation signal allows evaluation of the interconnected porosity of the material in fully-water-saturated condition. Moreover, since the higher relaxation rates at the pore walls increase the observed relaxation rates because of the high S/V ratio of the pore, it is possible to obtain information about dimensions of the ''pores'' and ''pore-size'' distributions through the distributions of relaxation times of the longitudinal (T_1) and transverse (T_2) components of the nuclear magnetization [1–3], even if major assumptions are usually required for the interpretation of experimental relaxation data, such as T_2 and T_1 relaxation curves, in terms of ''pore-size'' distributions [4].

It should be noted that the volume over which S/V is averaged by diffusion depends on local relaxation time and local (restricted) diffusion, so that the pore-size information is an average over a region that can be much larger than an individual pore, giving a local S/V. It is often useful to regard the local V/S as a pore dimension. If the pore space is heterogeneous only on a scale shorter than any local diffusion length, the relaxation will be single-exponential. Otherwise, the distribution of local V/S values will produce a distribution of relaxation times, and the relaxation will appear as a multiexponential decay. A T_2 process is always faster than a T_1 process, and, under favorable circumstances, the first one can give a better resolving power than the second, although it should be noted that the dephasing due to the presence of high instrumental and/or local magnetic fields gradients may be dominant in the transverse relaxation, masking the surface effects in such a way that T_2 distributions no longer represent the real local V/S distributions. In some particular cases, it is possible to correct the data to obtain information about the local V/S distributions also from T_2 measurements [4,5].

Magnetic resonance imaging (MRI) can be used for quantitative analysis [6]: water content and local V/S values can be evaluated in every internal region of a sample. Moreover, MRI of water is one of the main methods to get information on the distribution of a hydrophobic product in stone by direct visualization of the water diffused into the opaque medium [7–9]. Nevertheless, this accurate and spatially resolved methodology is usually suitable only for transportable objects with proper dimensions to fit into a standard laboratory imaging apparatus.

Recently, the possibility of using relaxation data as a non-destructive and non-invasive tool for *in situ* analysis of objects and materials of interest for the Cultural Heritage has become available, thanks to the development of portable surface probes [10,11], which can be applied to art objects of any dimensions, even if unmovable, simply by placing them on the selected surface of the sample to be analyzed [12–15].

The main drawbacks in the use of a portable NMR apparatus are the strongly inhomogeneous magnetic fields, which are due to the geometric features of such a single-sided device [5,11], and the low signal-to-noise ratio of measurements, which can be improved by increasing the number of signal acquisitions. Unfortunately, the intense instrumental magnetic field gradients make the transverse relaxation greatly influenced by molecular self-diffusion, causing the shifting of the distributions towards shorter values of T_2 in such a way that T_2 distributions no longer represent the ''pore-size'' distributions [4].

Unlike imaging, the relaxation approach is often a spatially non-resolved technique, but the use of a single-sided probe can provide information on the water content of a sample as a function of the depth. In fact, the instrument is equipped with interchangeable coils, which excite different fixed portions of the sample, namely the sensitive volume of the coil. Much effort is being made to enhance the analytical power of single-sided sensors for profiling capabilities [16] as well as imaging techniques [17,18].

In this work, experiments are carried out during the water uptake on samples of a highly porous biocalcarenite, Lecce Stone, untreated and treated with a chloroform solution of an acrylic resin able to change the wettability of the pore surfaces. For the treated samples, measurements have been performed during water uptake through the face of the sample opposite to the treated one and then, after drying the sample, through the treated one. In many cases [9], depending on the resin concentration and/or the treatment method, NMR measurements reveal that the untreated face is not significantly water repellent, because the hydrophobic product did not reach it (low penetration depth), while the treated face is usually highly water-repellent after short times of contact with the water source, but can allow water to penetrate during long exposure times. The aim of the present work is to quantitatively compare the results of the single-sided probe with those obtained by imaging to show features and advantages of the experimental methodologies, more than to discuss the performances of different treatments. For this reason, the results are focused on the comparison between the untreated sample and a treated one characterized by the highest water repellent properties.

By combining relaxometry and imaging we can obtain indirect information on the distribution of the polymer in the pore space and on the performance of the applied treatment at both pore and sample scales. Imaging clearly validates the interpretation of the results obtained by relaxometry. The work demonstrates that portable NMR devices can be successfully applied as non-destructive diagnostic techniques for *in situ* analysis of stone artifacts and for the determination of the performances of water-repellent treatments.

2. Materials and methods

The experiments were performed on Lecce Stone, a biocalcarenite having porosity $\varphi \approx 30\%$; samples were cut in slices of approximately $5 \times 5 \times 2$ cm^3. One sample was considered as reference, while the other was treated with a hydrophobic product widely employed for protection and/or reinforcement of stone artifacts: Paraloid B-72 (PB72), poly-(ethylmethacrylate/co-methylacrylate) 70/30. PB72 was applied as a chloroform solution (3% w/w) by capillary absorption (time of absorption 6 h) onto one of the two 5×5 cm^2 sides. All samples were dried at room conditions ($T = 25$ °C, $RH = 50$–60%) until constant weight was reached, and then their weights W_0 were measured.

The capillary water absorption was performed according to UNI 10859 [19]: each stone sample was placed, inside a closed box, on a pack 1 cm thick of filter paper (9 cm in diameter), soaked and submerged in distilled water up to approximately 0.5 cm.

For the water capillary absorption kinetics the stone samples, previously air-dried, were put in contact with the water source through the selected surface. Their weights $W = W_0 + W_W$ were measured at each absorption time during the imaging experiment.

Fully-water-saturated conditions were obtained by placing the air-dried samples in a vessel which was evacuated and then gradually filled with water.

The *in situ* NMR apparatus used for this work is the mq-ProFiler (Bruker Biospin, Italy). It is formed by two permanent magnets with a radio frequency coil placed in the space between them, all included in a volume of about $5 \times 5 \times 10$ cm^3, with a weight of about 2 Kg, while the portable electronics, to which the probe is connected, has a weight of about 10 Kg. The NMR single-sided probe used for exciting a layer within 0.2 cm from the magnet surface works at the Larmor frequency of 17.8 MHz. The sensitive volume of the surface coil is approximately $2.0 \times 0.2 \times 0.8$ cm^3. A probe working at 17.1 MHz was used for acquiring NMR signal from deeper volumes of the sample.

The single-sided NMR instrument was placed on the face opposite to that in contact with water, and the relaxation measurements were carried out at fixed absorption times during the water uptake without removing the equipment. This experiment allows both evaluating the changes of the hydration kinetics due to the action of the protective product and testing the performance of the instrument, which can be used for *in situ* measurements without taking away the samples from the water source.

For T_1 measurements (long, ~10 h) we have built up the longitudinal magnetization evolution by acquiring the spin-echo signal after each pulse sequence (saturation-τ_i-$\pi/2$-τ-π-acquisition) with different τ_i values, chosen in geometrical progression to cover the entire relaxation curve. The choice of saturating the longitudinal magnetization has been made to avoid too long a recovery time, and it has been obtained with a set of aperiodic $\pi/2$ pulses. Each signal was averaged over 512 acquisitions, and the shortest available half echo-time $\tau = 22$ μs to reduce T_2 effect was used.

Transverse relaxation data were acquired by the CPMG pulse sequence ($\pi/2$-τ-(π-τ-acquisition-τ-)$_n$) using the shortest half echo-time $\tau = 22$ μs to reduce the diffusion effect [4,5]. For every measurement of T_2 it has been necessary to acquire 8000 echoes to cover the entire relaxation curves.

Moreover, each sequence was repeated every 1 s for 1024 to maximize the signal-to-noise ratio, within a reasonable measurement time (~18 min).

Finally, the experimental data were processed with the UPEN algorithm, which gives the distributions of T_2 [2,3].

For the acquisition of the MR-images, the stone samples were taken away from the water source at each fixed absorption time and weighed. To minimize water evaporation during imaging measurements, each stone was wrapped up in a plastic film that, as previously checked, does not contribute to the NMR signal.

^{1}H-MRI images were acquired at room temperature by means of ARTOSCAN™ (Esaote S.p.A., Genova, Italy), consisting of a 0.2 T permanent magnet corresponding to 8 MHz for protons. Multi-slice spin-echo [6] sequences were used to obtain 10 axial sections on each sample (slice thickness = 5 mm, gap between slices = 1 mm, pixel size = 0.78×0.78 mm^2, number of excitations = 8, repetition time TR = 900 ms, echo time $2\tau = 10$ ms). Particular care was devoted to avoid electronic saturation of the signal and to guarantee that from sample to sample the signal intensity was determined on the same dynamic range.

Images were analyzed with ARTS, in-house software for Windows platform, developed using the C++ language and the MFC framework (Microsoft), that allows managing the images obtained from the tomograph ARTOSCAN. Images created and displayed by ARTOSCAN are usually normalized to obtain best visualization and contrast. To make different images quantitatively comparable with each other, ARTS brings back the images at their original absolute value, by using the necessary information contained in the header of the original image. Then, the software is able to display the images and their histograms, with many kinds of different weightings, and to compute signal intensity averages on user-defined Regions of Interest (ROIs). In this work, rectangular ROIs (about 2 cm × 2 mm) were chosen to select layers (L_k, with $k = 1, \ldots, 8$) at different depths in the sample, and the corresponding average signal intensities I_k were computed.

Since the aim of this paper is to show advantages of the experimental methodology more than to discuss the performances of different treatments [9], the results here reported are devoted to a comparison between the untreated sample and the treated sample (478 mg of PB72 in 3% (w/w) chloroform solution) characterized by the highest water repellent performance.

3. Results and discussion

Fig. 1a reports T_1 distributions obtained by UPEN from the fully-water-saturated reference sample. Closed symbols are for a sensitive volume 2 mm thick near the surface, acquired with the single-sided apparatus. For comparison, the results obtained on a small sample (cylinder having diameter 7 mm, height 7 mm) by a standard laboratory relaxometer operating at 20 MHz (open symbols) are shown. A very good agreement is observed.

Fig. 1b reports T_2 distributions obtained by UPEN from the fully-water-saturated reference sample. Again, open symbols are for the data acquired with the laboratory relaxometer, while closed symbols are for four sensitive volumes located at different depths, acquired with the single-sided apparatus. Actually, a depth of about 1 cm can be reached, in different experimental conditions, by simply changing the probe. The four curves of Fig. 1b were obtained by using two different probes, giving a sensitive volume in a ~2 mm thick layer, centered at ~1 mm and at ~3 mm from the surface, respectively, and applied on the two 5×5 cm^2 opposite surfaces of the sample (S_1 and S_2). The ability of the single-sided device to select signals at different depths allows one to observe the variability of the water saturation and of the pore-space structure (shape of the distribution function) with the sensitive volume location. The T_2 distributions are broad, covering the range between 0.1 ms and 1000 ms, and suggest the presence of micro-porosity; some macroscopic heterogeneity of the rock is suggested by some of the single-sided measurements, in particular in the region of the micro-porosity. The shift to shorter times with respect to the distribution obtained with the standard relaxometer is due to the highly inhomogeneous field of the single-sided device. It has been demonstrated that this does not affect the T_1 data [4,15].

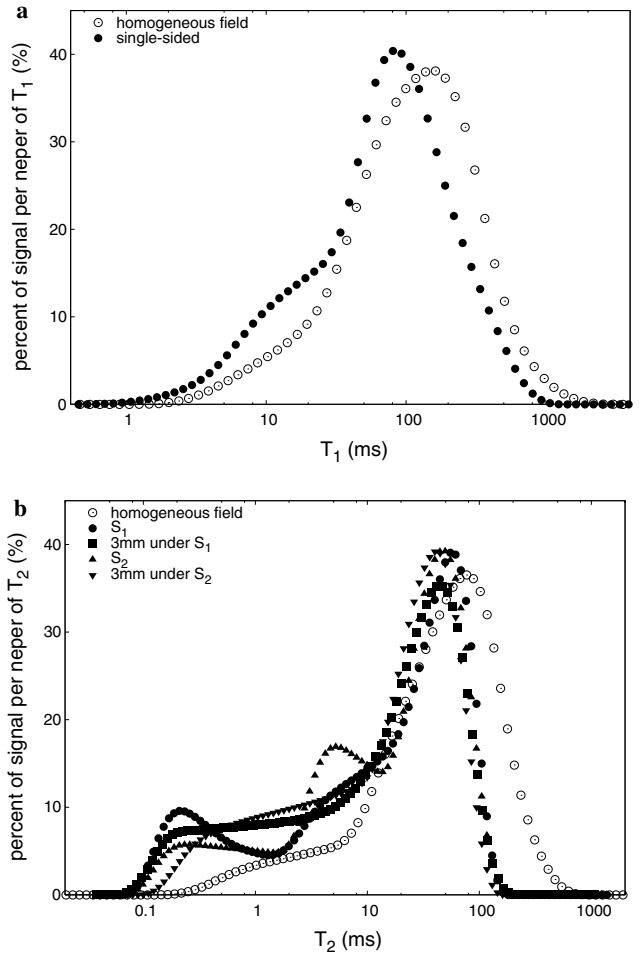

Fig. 1. T_1 (a) and T_2 (b) distribution functions for the fully-water-saturated untreated sample. The ordinate is computed as an approximation to $(dM)/(d \ln T_{1,2})$, where M is percent of the total extrapolated signal. Equal areas correspond to equal fractions of the total signals. The NMR signals have been acquired in homogeneous external magnetic fields (open symbols) at $\nu_0 = 20.0$ MHz and in the inhomogeneous external magnetic fields of the single-sided device (closed symbols) at $\nu_0 = 17.8$ MHz. In (b) the closed symbols refer to signals acquired at different depths of the sample by placing the single-sided instrument on the two opposite 5×5 cm^2 faces (S_1 and S_2, S for "Surface") of the sample and/or by simply changing the coil. For acquiring NMR signal from the volumes centered at 3 mm inside the sample a probe working at 17.1 MHz was used.

In this work T_2 measurements were preferred to T_1 because of the shorter measurement duration and because T_2 values give the chance of a molecular probe with a larger resolving power than T_1 [4]. Moreover, we are interested in the changes of the distributions before and after treatment [20], more than in the distribution themselves. In any case, the use of a very short half echo-time for CMPG experiments guarantees that the de-phasing effect is greatly reduced.

The water uptake kinetics in the sensitive volume can be followed over the course of time without interrupting the absorption process, simply by keeping the device on the opposite surface during the absorption. In this experiment the ^{1}H signal was detected from the same sensitive volume in a layer of about 2 mm below the surface opposite to that in contact with the water source.

Fig. 2 shows the results for the reference sample. The distributions of T_2 data are shown in 3D representation. Within the first hour of absorption no signal amplitude is detected near the un-wetted surface; only after 1 h a very small signal amplitude is revealed at shorter relaxation times (T_2 in the range $0.1 \div 1$ ms), which corresponds to the signal from the smallest pores and/or from larger pores only partially filled. At longer absorption times (~2 h) the signal amplitude increases, the distributions are shifted towards larger values of transverse relaxation times, and their shapes are closer and closer to that observed in fully-water-saturated conditions, because in the course of time the amount of water near the analyzed surface increases, and larger pores are gradually filled. The shift to larger relaxation times reflects the increasing mixing by diffusion of water between adjacent pores and/or to the progressive ingress of water in pores previously only partially filled. The results for the treated sample are reported in Fig. 3. For this sample two different conditions were used. After the first absorption through the untreated face, the sample

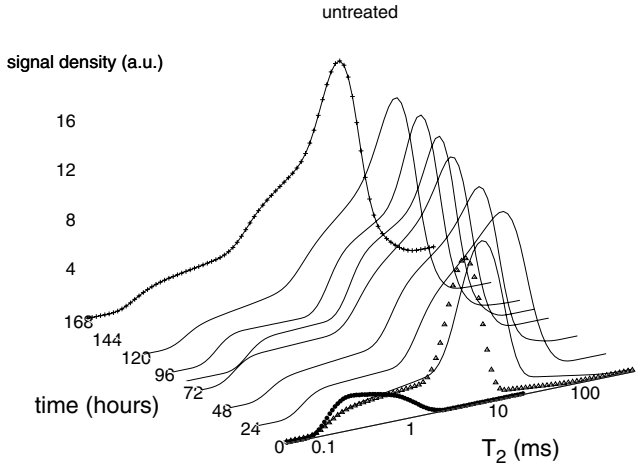

Fig. 2. 3D visualization of the time evolution of the T_2 distribution during the water uptake of the untreated sample from a $5 \times 5\ cm^2$ face, with no signal observed before 1 h. The decay signals have been acquired with the single-sided device from a layer of about 2 mm near the surface opposite to that in contact with the water source. [1 h (●), 2 h (△), 3 h ÷ 120 h (—), 168 h (+)].

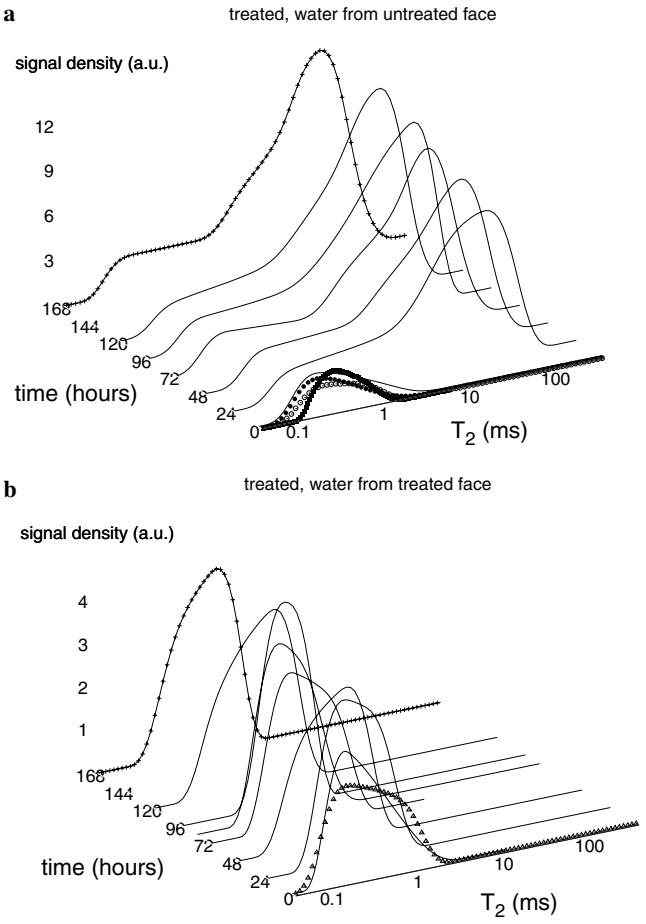

Fig. 3. As in Fig. 2, for the treated sample for water absorption through the untreated (a) and the treated faces (b). [0 h (■), 0.2 h (○), 1 h (●) 2 h (△), 3 h ÷ 120 h (—), 168 h (+)].

was dried in air to constant weight, and the experiment was repeated through the treated face. In this way, the results available with mq-ProFiler can furnish a complete description of the efficacy of the water-repellent product. During the first 3 h of absorption through the untreated face (Fig. 3a), the signal amplitude is less than for the reference sample, with a broad peak in the range $0.1 \div 1$ ms. Unlike that for the reference, the shift to larger values of T_2 at increasing absorption times is not gradual. No significant differences are observed between 0 and 3 h. After 1 day the shape of the distribution has approached the final one. This result shows that initially the capillary rise of water is reduced by the hydrophobic product and limited to smaller pores or to larger ones only partially filled with water. However, after the first hours of absorption, the water molecules find a way through the polymeric barrier and can invade all the pore space available at normal pressure conditions.

A different behavior is observed when the absorption face is the treated one. The T_2 distributions (Fig. 3b), detectable only after 2 h, are limited to only the region of smaller T_2 values for every absorption time.

A strange signal was detected in the treated sample in the first minute of water absorption through its untreated face when the measured face was the treated one (Fig. 3a). A similar signal was absent in the same sample during the water uptake through its treated face when the measured face was the untreated one (Fig. 3b), as well as in the reference sample (Fig. 2). An explanation is that the signal observed may be due to the water entrapped by the hydrophobic product very near the treated surface and not evaporable at room conditions. To confirm this hypothesis, the treated sample was dried under vacuum for 1 day and its treated surface measured again. In this case the signal amplitude was indistinguishable from noise (data not shown).

Finally, the single-sided data can be compared with the gravimetric data. The areas under the UPEN distributions give the total signals extrapolated to zero time and should be proportional to the masses of water in the pore spaces inside the sensitive volumes. As a matter of fact, as has been just mentioned, the unilateral device is characterized by a natural spatial selectivity of the sensitive volume of the probe that allows one to measure the NMR parameters in a precise and fixed volume of the sample. That makes it possible, by utilizing proper calibration procedures [14], to relate the NMR magnetization to the water content of this volume.

In Fig. 4a the mass of water absorbed by a sample (W_W) and the extrapolated equilibrium magnetization (M_0) obtained by UPEN in the sensitive volume are plotted against absorption time. Even though the relaxation data refer to the sensitive volume and the gravimetric data to the entire sample volume, a comparison between the two sets of data can be useful. In particular, the gravimetric data of the treated sample confirm some features of the relaxation data: a very low water uptake from the treated face (circles) and a high water uptake from the untreated face (triangles), comparable with the water uptake of the untreated sample (squares). As

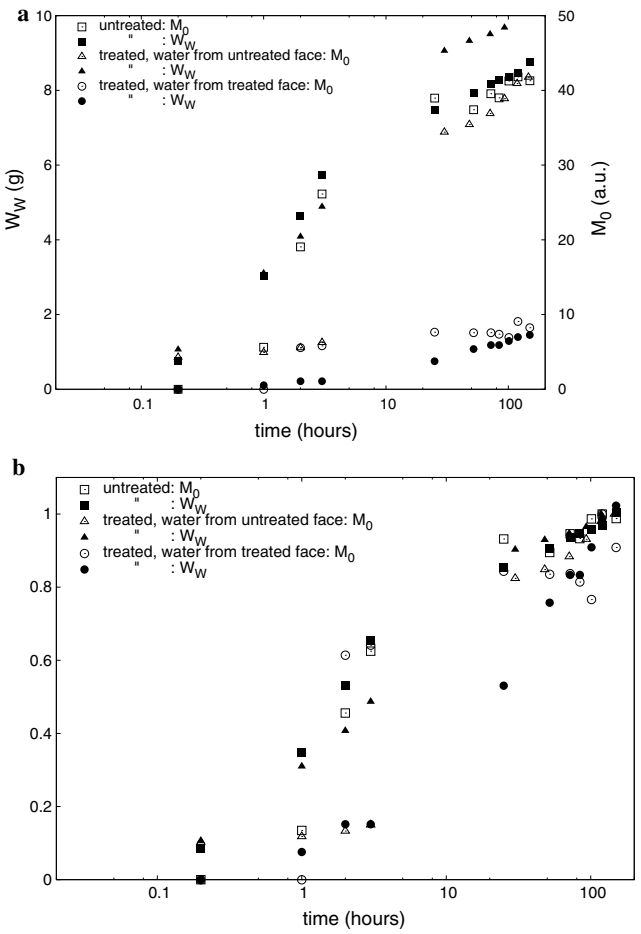

Fig. 4. Comparison between gravimetric and relaxation data during the water uptake for the untreated sample and for the treated one, through its untreated and treated faces. In (a) the mass of water, W_W, absorbed by the sample and the extrapolated equilibrium magnetization, M_0, in arbitrary units, obtained by UPEN in the sensitive volume, are plotted against the time. In (b), the data of (a) are shown after normalization to their asymptotic values.

shown by Fig. 3a and b, measurements performed keeping the device on the treated face of the sample during water absorption through the face opposite to the treated one show that the untreated face is not strongly water repellent. In such conditions, liquid water has been able to penetrate into the sample, though with kinetics slower than observed in the untreated sample. To better visualize the kinetics, in Fig. 4b the same data reported in Fig. 4a are represented after normalization of each value to the corresponding asymptotic value. Finally, measurements performed on the treated sample with absorption through the treated face demonstrate that it is highly water-repellent but can allow small amounts of water to penetrate at long exposure times. It may be noted from Fig. 4a that about 85% of the small final amount of water entering through the treated face (circles) reaches the sensitive region on the opposite face in 2 or 3 h, at which time the overall sample weight has increased only 20% of the small final amount. On the other hand, water entering through the untreated face (triangles) does not give any more signal in 2 or 3 h than through the treated face but adds far more to the sample weight. This appears to suggest that the larger pores throughout much of the sample have become somewhat water repellent, while the smaller pores are not much affected, because of the high molecular weight of the polymer. When water enters through the treated face (where a higher concentration of polymer is present), it can enter only very slowly, but a small amount may be transported rapidly through the smaller pores to the opposite face without significantly filling the larger pores in the time of the experiment, whereas water can enter fast enough through all the pores of the untreated face to fill also some of the larger pores before much reaches the opposite face.

MR-images of internal sections of the two samples, acquired during water capillary absorption, show water distributions consistent with the results obtained by the single-sided device. Fig. 5 reports images of the central slices of the untreated sample (a), of the treated one with absorption through the untreated face (b), and through the treated face (c). In Fig. 5a the time sequence of images acquired from the reference sample shows a very good agreement with the results of the relaxation measurements on the same sample (Fig. 2). Moreover, imaging results confirm the homogeneous distribution of the water throughout the whole sample. The images of Fig. 5b show that after 24 h it has been possible to detect the presence of water in the whole sample, as proved by single-sided experiments (Fig. 3a). The penetration of the acrylic polymer is evident. The images of Fig. 5c at 1 h, 24 h as well as after 168 h (7 days) appear completely dark, since only water with T_2 less than the 10 ms necessary to show in the imaging is present, as can be seen in Fig. 3b. Thus, also in this case, the results obtained with imaging are in good agreement with the information given by the single-sided probe (Fig. 3b).

Imaging data have been analyzed by the software ARTS (see Section 2) to quantitatively evaluate the amounts of observable water in different positions inside the sample. In Fig. 6 the time evolution of the signal intensity, roughly proportional to the amounts of water, at different depths in the central sections of the samples during water absorption for the reference sample (a) and for the treated sample through its untreated face (b) are shown. The quantity (I) has been expressed as the integral of the signal intensity of eight consecutive layers $L_1, L_2, \ldots, L_8$, of about 2 mm each, for increasing distances from the surface in direct contact with the water, chosen in such a way as to cover all the thickness of the sample. The signal intensities are $I_k(t)$, where $k = 1, \ldots, 8$ is the layer index. $I_k(t)$ values are compared with the signal intensities (M_0) measured at the same absorption times at the top of the samples by the single-sided device (closed symbols). Obviously, the relaxation data refer approximately to the layer L_8, which in the image is the farthest from the layer L_1 in direct contact with water.

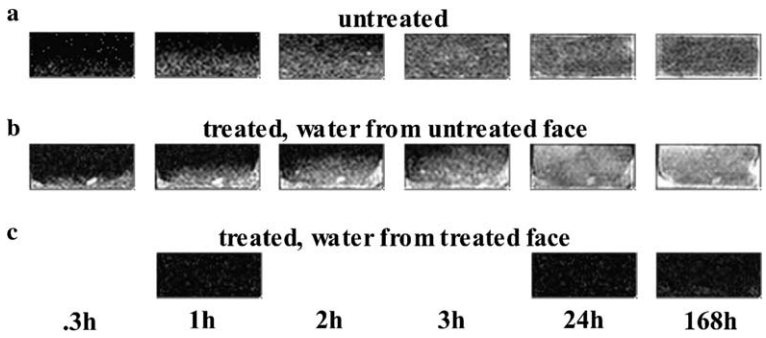

Fig. 5. MR-images of an internal section of the reference sample (a) and of the treated one during the water absorption up to 168 h (7 days). For the treated sample, the absorption has been through the untreated (b) and treated faces (c).

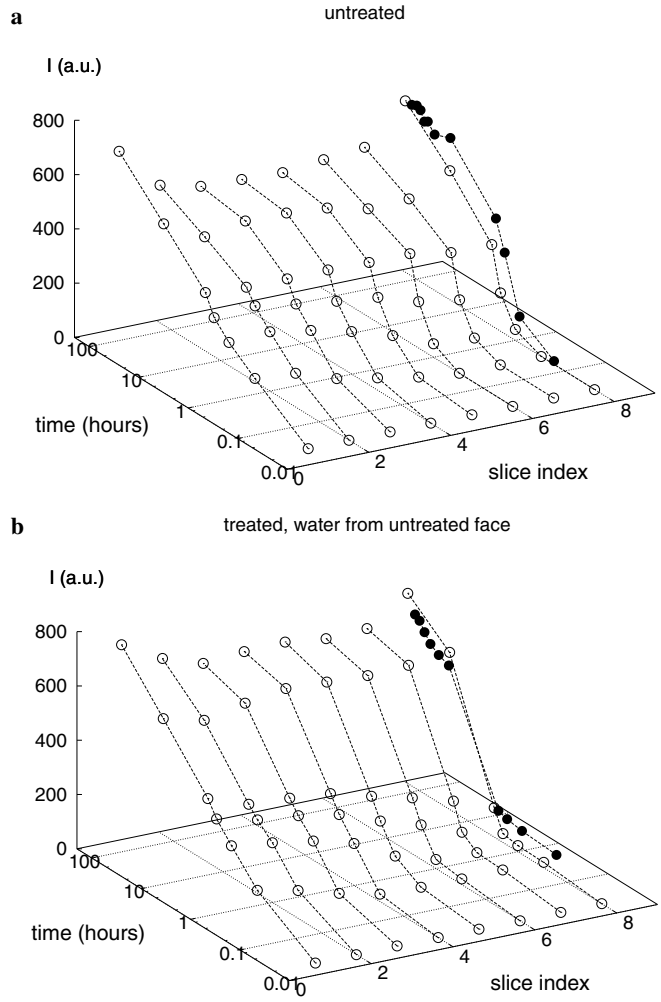

Fig. 6. Time evolution of the water uptake during water absorption of the untreated sample (a) and of the treated one through its untreated face (b). The water amounts have been obtained from the images of Fig. 5(a) and (b) and have been expressed as the integrals of the pixel signal intensity, $I_k(t)$, of slices $(L_1, L_2, \ldots, L_8)$ of about 2 mm at increasing distances from the absorbing surface. L_1 is the layer in direct contact with the water. For comparison, the single-sided signal intensities (magnified 15×) measured on the face opposite to the absorption, as in Fig. 4a, have been also reported (closed symbols).

The behavior of the data reported in Fig. 6a and b with increasing index of the layers is consistent with the expected absorption kinetics. The lower values of the signal at the longest absorption times for the untreated sample, with respect to those for the treated sample, are consistent with the lower masses of water absorbed by the untreated sample, obtained by weighing the samples (see Fig. 4a). Focusing attention on the imaging data at the longest absorption time, it is evident that the external surfaces (L_1 and L_8) of both samples exhibit higher intensities than the internal layers. This result is expected to be due to boundary effects, rather than to image artifacts or gross sample inhomogeneity. To validate such interpretation, an image of the untreated sample water-saturated under vacuum has been performed (image not shown). This different hydration mechanism ensures that all the pores are now completely filled by water. With the aim to compare the absorptions at normal pressure and under vacuum, the behavior of the equilibrium intensities, $I_k(\infty)$ (after ~7 days of water capillary absorption), relative to the different layers in the samples is compared for the two hydration methods. To better show the dispersion of the integrals of pixel intensities at different depths in the sample, we form the intensity fluctuation function $I_k(\infty) - I_M$ where $I_M = \Sigma_k(I_k(\infty))/8$. Moreover, to better compare the functions for different samples, the relative fluctuations, $(I_k(\infty) - I_M)/I_M$ were computed. In Fig. 7, the behavior of $(I_k(\infty) - I_M)/I_M$, of both reference and treated samples, are reported in comparison with the results obtained for the same untreated stone, saturated under vacuum. While in this last case the untreated rock exhibits only minor fluctuations of values around zero, in water capillary absorption conditions the intensity of fluctuation is larger for the external layers than for interior ones, with a well reproducible and symmetric feature for both treated and untreated samples. This result confirms that larger amounts of water fill the pore space near the external surfaces than in the inner layers. An interpretation could be that in the surface layers air can be easily removed by the water and does not remain trapped in the pore space, as happens in the internal regions of the sample.

To further check the goodness of the quantitative analysis of the images, the data obtained by the images of the central section of the samples in the course of time were fitted to the Washburn model for capillary rise. The Washburn equation [21], originally derived for a liquid rising

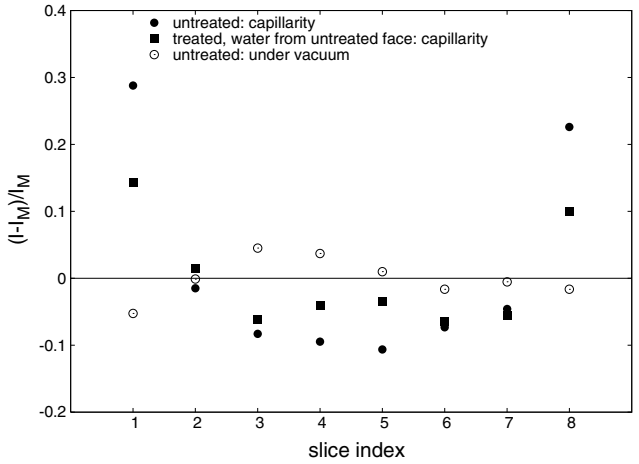

Fig. 7. Relative fluctuation of the integral of the equilibrium pixel intensity, $(I_k(\infty) - I_M)/I_M$, after 168 h of capillary water absorption obtained from the last MR-images of Fig. 5 (a) and (b), compared with the corresponding data obtained for the reference sample after full water saturation under vacuum (image not shown). For each set of data, I_M is the average of the integrals of the pixel equilibrium intensities of the eight slices.

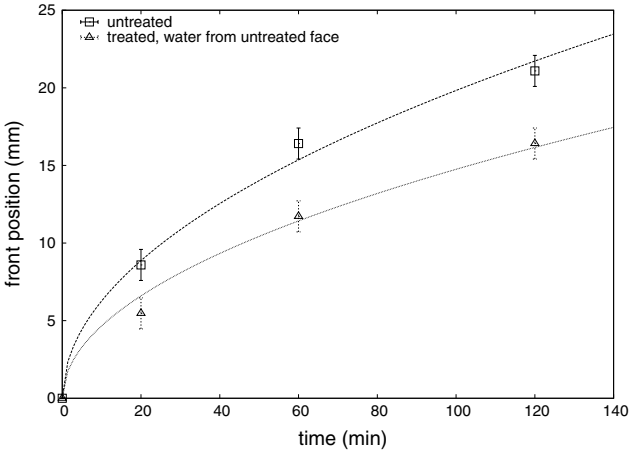

Fig. 8. Position z of the front in the first 2 h of water uptake, computed by ARTS from the images of Fig. 5(a) and (b), by assuming $z = 0$ at the absorption interface. Open squares are for the untreated sample, open triangles are for the treated sample. The plotted curves are the best fits to Eq.2, giving a significantly larger *sorptivity* value for the untreated ($S = 1.98$ mm/(min)$^{1/2}$) than for the treated sample ($S = 1.48$ mm/(min)$^{1/2}$).

in a cylindrical capillary tube, is frequently used to describe the phenomenon of the capillary rise in porous media [22]:

$$t(z) = \frac{\theta_s h_e}{k_s} \ln\left(\frac{h_e}{h_e - z}\right) - \frac{\theta_s z}{k_s} \quad (1)$$

where z is the height of the wetting front, θ_s is the saturated water content, k_s is the saturated hydraulic conductivity, h_e is a parameter typically corresponding to the equivalent saturated height of the cumulative mass absorbed (in a capillary tube, the equilibrium height), and t is time. The equation corresponds to macroscopic water absorption in porous media with the assumption of an abrupt interface between the wet and dry regions and complete saturation of the wetted region (Green and Ampt [23] model).

For small values of z the Eq. (1) is simplified [24]:

$$z = S\sqrt{t} \quad (2)$$

where S is called *sorptivity* and expresses the capacity of a porous medium for capillary uptake of a liquid. In general it is a crude approximation, as saturation gradients are clearly present, as well shown in Fig. 6a and b. Nevertheless, we will see that also our data satisfy Eq. (2). In the images of Fig. 5a and b, the position z of the front, by assuming $z = 0$ at the absorption interface, was evaluated at the position of the layer L_k where the signal intensity abruptly changed, going to the level of the noise.

Fig. 8 shows the z coordinate of the front for the untreated and treated sample (absorption from the untreated face). The best fit of the data to Eq. (2) is reasonably good and gives $S = 1.98$ mm/(min)$^{1/2}$ and $S = 1.48$ mm/(min)$^{1/2}$ for the untreated and treated samples, respectively. Experiments performed on a new set of samples, where a larger number of data were acquired during the absorption time, by using faster image acquisition sequences, confirmed the feasibility and the reliability of the method to follow in a quantitative non-destructive way the mechanisms of the ingress of water inside an opaque sample.

4. Conclusions

The ability of NMR techniques such as relaxometry and imaging to detect the presence of water and to quantify structural properties of the pore-space, such as porosity and pore-size distributions, and effects of environmental damage and changes of capillary water absorption properties due to hydrophobic treatments, makes low-resolution NMR techniques unique and irreplaceable diagnostics tools for porous materials, especially in the field of the Cultural Heritage.

In this paper, the potentialities of different NMR investigations has been tested by following the kinetics of water uptake on samples of a biocalcarenite, Lecce Stone, with and without a water-repellent treatment with Paraloid B-72, an acrylic resin frequently employed for reinforcing and/or protective treatments of building materials.

A portable single-sided NMR device and a laboratory imaging apparatus were used. The analysis with the surface probe is different from that performed with the imaging technique, which allows one to visualize the amount of water with T_2 long enough for the particular imager everywhere inside the porous material and to see the variation with position of the effects of the hydrophobic polymer. On the other hand, the single-sided apparatus can give information at the pore scale, from large and small pores, with the possibility of spatial selection of the sensitive volume.

Relaxation time distributions obtained with the portable single-sided device and images obtained by the fixed homogeneous-field laboratory MRI instrument were quantitatively compared. It has been shown that the single-sided

devices can quantify water saturation at the pore scale in well-defined sensitive volumes. Images can be quantitatively analyzed to get the water content in selected regions of interest in each section of a sample. The paper gives a clear demonstration of the synergetic improvement in our understanding of water absorption kinetics in treated and untreated stone samples, thanks to the combined use of non-destructive relaxometry and imaging. While imaging allows one to get information on the effects of the polymer at the sample-scale, relaxation data give information on the effects of the polymer at the pore-scale.

As a matter of fact, the visualization of water and the quantitative data obtained by imaging at different absorption times support the interpretation of the changes of the relaxation time distributions obtained by *in situ* relaxometry.

In conclusion, both NMR imaging and portable relaxation devices have features that make their combination a unique tool for Cultural Heritage applications. In particular the portable device, having a single-sided geometry, can be successfully applied as a non-destructive tool for *in situ* analysis of pore space structure and water uptake for different treatment conditions.

Acknowledgments

Some of us (P.F., V.B.) thank ESAOTE S.p.A. for assistance in digital images processing and FIRB 2001. The authors thank R.J.S. Brown for useful discussions and Mirko Gombia for imaging acquisition.

References

[1] VV AA, Proceedings of the Seventh International Conference on Recent Advances in MR Applications to Porous Media, Eds. P. Fantazzini, J.H. Gore, J.P. Korb, Magn. Reson. Imaging, 23 (2005) 121–444. For the previous MRPM conferences see the special issues: Magn. Reson. Imaging 9 (1991) 639–888; 12 (1994) 161–378; 14 (1996) 697–1006; 16 (1998) 449–714; 19 (2001) 291–593; 21 (2003) 159–450.

[2] G.C. Borgia, R.J.S. Brown, P. Fantazzini, Uniform-penalty inversion of multiexponential decay data, J. Magn. Reson. 132 (1998) 65–77.

[3] G.C. Borgia, R.J.S. Brown, P. Fantazzini, Uniform-penalty inversion of multiexponential decay data II: data spacing, T2 data, systematic data errors, and diagnostics, J. Magn. Reson. 147 (2000) 273–285.

[4] C. Casieri, F. De Luca, P. Fantazzini, Pore-size evaluation by single-sided nuclear magnetic resonance measurements: compensation of water self-diffusion effect on transverse relaxation, J. Appl. Phys. 97 (4) (2005) 043901–043910.

[5] C. Casieri, S. Bubici, F. De Luca, Self-diffusion coefficient by single-sided NMR, J. Magn. Reson. 162 (2003) 348–355.

[6] P.T. Callaghan, Principles of Nuclear Magnetic Resonance Microscopy, Oxford Science Publcations, New York, 1991.

[7] G.C. Borgia, M. Camaiti, F. Cerri, P. Fantazzini, F. Piacenti, Study of water penetration inside rock materials by nuclear magnetic resonance tomography: hydrophobic treatment effects, J. Cultural Heritage 1 (2000) 127–132.

[8] G.C. Borgia, V. Bortolotti, M. Camaiti, F. Cerri, P. Fantazzini, F. Piacenti, Performance evolution of hydrophobic treatments for stone conservation investigated by MRI, Magn. Reson. Imaging 19 (2001) 513–516.

[9] G.C. Borgia, M. Camaiti, F. Cerri, P. Fantazzini, F. Piacenti, Hydrophobic treatments for stone conservation: influence of the application method on penetration, distribution, and efficiency, Stud. Conserv. 48 (2003) 217–226.

[10] G. Eidman, R. Savelsberg, P. Blümler, B. Blümich, The NMR MOUSE, a mobile universal surface explorer, J. Magn. Reson. 122 (1996) 104–109.

[11] F. Balibanu, K. Haiulu, R. Eymael, D.E. Demco, B. Blümich, Nuclear magnetic resonance in inhomogeneous magnetic fields, J. Magn. Reson. 145 (2000) 246–258.

[12] I. Viola, S. Bubici, C. Casieri, F. De Luca, The Codex Major of the Collectio Altaempsiana: a non-invasive NMR study of paper, J. Cultural Heritage 5 (2004) 257–261.

[13] C. Casieri, S. Bubici, I. Viola, F. De Luca, A low resolution non-invasive NMR characterization of ancient paper, Solid State NMR 26 (2004) 77–85.

[14] C. Casieri, L. Senni, M. Romagnoli, U. Santamaria, F. De Luca, Determination of moisture fraction in wood by mobile NMR device, J. Magn. Reson. 171 (2004) 363–372.

[15] M. Brai, M. Camaiti, C. Casieri, F. De Luca, P. Fantazzini, A. Maccotta, F. Morreale, C. Terenzi, From laboratory to in-situ nuclear magnetic resonance diagnostics: an application to building materials of the greek-roman theatre of Taormina, in: 8th International Conferences on Non-destructive Testing and Microanalysis for the Diagnostics and Conservation of the Cultural and Environmental Heritage, 15–19 May 2005, Lecce, Italy (2005) ISBN 88-89758-00-7.

[16] J. Perlo, F. Casanova, B. Blümich, Profiles with microscopic resolution by single-sided NMR, J. Magn. Reson. 176 (2005) 64–70.

[17] J. Perlo, F. Casanova, B. Blümich, 3D imaging with a single-sided sensor: an open tomograph, J. Magn. Reson. 166 (2004) 228–235.

[18] R. Cignini, R. Melzi, F. Tedoldi, C. Casieri, F. De Luca, Large surface mapping by unilateral NMR scanner, Magn. Reson. Imaging (2006), doi:10.1016/j.mri.2006.03.005.

[19] UNI 10859, Norma Italiana Beni Culturali, Materiali lapidei naturali e artificiali, 'Determinazione dell'assorbimento d'acqua per capillarità', January 2000.

[20] L. Appolonia, G.C. Borgia, V. Bortolotti, R.J.S. Brown, P. Fantazzini, G. Rezzaro, Effects of hydrophobic treatments of stone on pore water studied by continuous distribution analysis of NMR relaxation times, Magn. Reson. Imaging 19 (2001) 509–512.

[21] E.W. Washburn, The dynamics of capillary flow, Phys. Rev. 17 (1921) 273–283.

[22] D.A. Lockington, J.Y. Parlange, A new equation for macroscopic description of capillary rise in porous media, J. Colloid Interface Sci. 278 (2004) 404–409.

[23] W.H. Green, G.A. Ampt, Studies on soil physics, 1: The flow of air and water through soils, J. Agric. Sci. 4 (1911) 1–24.

[24] M. Lago, M. Araujo, Capillary rise in porous media, J. Colloid Interface Sci. 234 (2001) 35–43.